Pressure-induced Jahn-Teller suppression in $Rb_2CuCl_4(H_2O)_2$: Pseudo-Jahn-Teller effect

F. Aguado,[1] F. Rodríguez,[1,*] R. Valiente,[2] J. P. Itié,[3,4] and P. Munsch[4]

[1]*DCITIMAC, Facultad de Ciencias, Universidad de Cantabria, Santander 39005, Spain*
[2]*Departamento de Física Aplicada, Universidad de Cantabria, Santander 39005, Spain*
[3]*Université Pierre et Marie Curie, B77 4 Place Jussieu 75252 Paris Cedex 05, France*
[4]*LURE, Université Paris-Sud, BP34, 91898 Orsay Cedex, France*

In this work we investigate the variation of the local structure around Cu^{2+} as well as the crystal structure in $Rb_2CuCl_4(H_2O)_2$ through x-ray absorption spectroscopy (XAS) and x-ray diffraction (XRD) as a function of pressure. We show that the application of pressure induces a local structural change in the Jahn-Teller (JT) $CuCl_4(H_2O)_2^{2-}$ complex from an axially elongated complex to a compressed one, yielding disappearance of the JT distortion related to the four in-plane Cl^- ligands, which are responsible for the antiferrodistortive structure displayed by the crystal at ambient pressure. According to the Pseudo-Jahn-Teller (PJT) theory (electron-phonon coupling $E \otimes e$), the presence of water ligands enhances the JT release at pressures well below the metallization pressure. The results are compared with recent pressure experiments on A_2CuCl_4 layered perovskites and heteronuclear $CuCl_4L_2$ complex series, L :$Cl \rightarrow H_2O \rightarrow NH_3$, and explained on the basis of the PJT model.

PACS number(s): 64.70.Kb, 62.50.+p, 61.50.Ks, 61.10.−i

I. INTRODUCTION

The presence of $Cu^{2+}(3d^9)$,[1–9] $Mn^{3+}(3d^4)$,[9–14] or $Cr^{2+}(3d^4)$ (Refs. 15–17) ions either as a constituent or impurity in insulating materials gives rise to a great variety of coordination geometries, even if the impurity is placed in cubic sites. This is a direct consequence of the Jahn-Teller (JT) effect related to the e_g hole or electron ground state.[1,2,18–20] In hexacoordinated systems of either homonuclear MX_6 (M =$Cu, Cr, Mn; X=H_2O, NH_3, O, F, Cl, Br$) or heteronuclear MX_4L_2 ($X=O, F, Cl, Br; L=H_2O, NH_3$), the observed coordination geometries mostly correspond to low-symmetry elongated octahedra. The occurrence of an elongated geometry can be explained on the basis of electron-phonon coupling between octahedral E_g electronic states and e_g vibrations: $E \otimes e$ JT model. The knowledge of a given symmetry around the JT ion is important since both the distortion and the packing of JT complexes strongly influence the optical, electrical, and magnetic properties of these materials. Hence the establishment of structural correlations is crucial for a microscopic materials characterization.[1,2,5,7,11–15,21]

The $E \otimes e$ model predicts coordination geometry variations in homonuclear MX_6 JT complexes from elongated to compressed passing through different rhombic intermediates, or even suppression of the JT distortion, applying axial stress or hydrostatic pressure. However no clear evidence of this effect was reported so far using local probes, in spite of the intense activity to achieve this phenomenon using high-pressure techniques.[22,23] In fact, pressure-induced phase transitions observed in $[C_2H_5NH_3]_2CuCl_4$ by Raman and optical spectroscopy was initially ascribed to structural changes associated with the suppression of the JT distortion.[23] But structural studies performed by x-ray absorption (XAS) and x-ray diffraction (XRD) techniques in the isostructural $[C_3H_7NH_3]_2CuCl_4$ compound showed that indeed such transformations are mainly related to tilts of the $CuCl_6^{4-}$ octahedra rather than to the JT suppression.[22] Also recent structural studies under pressure in $LaMnO_3$ using XRD (Ref. 24) or neutron diffraction (ND) (Ref. 25) report controversial results on pressure effects of the JT distortion.

In general, pressure results give evidence of the tendency of $CuCl_6$ or MnO_6 to preserve their *molecular character* associated with the JT distortion. In $CuCl_6$, it is due to the higher compressibility of the crystal with respect to the local compressibility, whose molecular stiffness is enhanced by the additional JT binding energy of about 0.25 eV.[8] Recent results on $NaMnF_4$ under pressure also support this idea.[13]

In this work, we investigate the local structure of homo- and heteronuclear $CuCl_4L_2$ (L:Cl, H_2O, NH_3) systems on the basis of the pseudo-Jahn-Teller (PJT) model;[26] the electron-phonon coupling is treated in the same manner as homonuclear octahedral complex ($E \otimes e$), but introducing additional strain terms to describe both the effect of the axial L ligands and the crystal anisotropy. Interestingly, the PJT model can explain the observed coordination geometry of homo- and heteronuclear Cu^{2+} systems, as well as its changes induced by stress, hydrostatic pressure or placing the JT ion in low-symmetry sites in impurity systems. In this way, the elongated-octahedron geometry observed for $CuCl_6$ in the Cu^{2+}-doped NaCl (Ref. 27) and $CsCaCl_3$ (Ref. 28) (3D cubic) crystals and the A_2CuCl_4 (Refs. 7,8) or Cu^{2+}-doped A_2CdCl_4 (Refs. 7,29,30) (2D layer perovskites) crystals forming antiferrodistortive (AFD) structures can be explained on the basis of the PJT model taking into account the axial-stress field is due to the crystal anisotropy. On the other hand, the heteronuclear $CuCl_4(H_2O)_2^{2-}$ complex, which form intraplane ferrodistortive (FD) and interplane AFD structure associated with the axially-elongated of one Cl-Cu-Cl axis in the $Rb_2CuCl_4(H_2O)_2$ crystal (Fig. 1),[31] appears to be stabilized within this model by the ligand-field stress of the water molecules. However the axially-
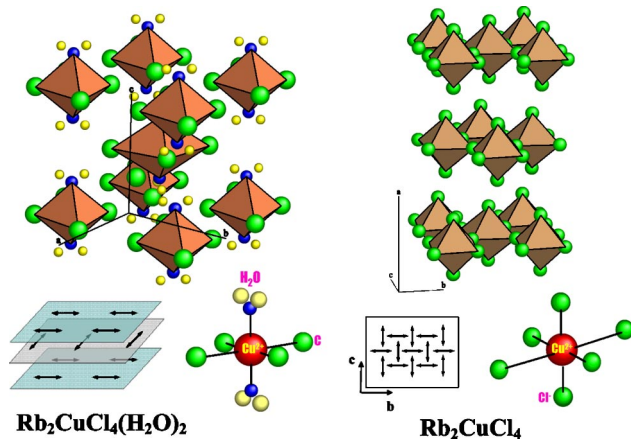
Rb$_2$CuCl$_4$(H$_2$O)$_2$ **Rb$_2$CuCl$_4$**

FIG. 1. (Color online) Crystal structure of Rb$_2$CuCl$_4$(H$_2$O)$_2$ ($P4_2/mnm$) and Rb$_2$CuCl$_4$ ($Cmca$). Only the Cu complexes displaying an AFD structure are depicted. Note the different AFD structure displayed by each crystal: intralayer-FD and interlayer-AFD for Rb$_2$CuCl$_4$(H$_2$O)$_2$ whereas intralayer-AFD for Rb$_2$CuCl$_4$. The arrow indicates the complex elongation.

compressed geometry in the CuCl$_4$(NH$_3$)$_2^{2-}$ complex occurs by the stronger ligand field of the ammonia molecules.[32,33]

The two-dimensional Rb$_2$CuCl$_4$(H$_2$O)$_2$ compound offers the possibility of exploring structural change from the rhombic-elongated geometry to the tetragonal-compressed one by applying pressure. The PJT model foresees the occurrence of such a transition in the CuCl$_4$(H$_2$O)$_2^{2-}$ complex at a weaker axial stress than the transition stress required for homonuclear CuCl$_6^{4-}$ complexes. The presence of water molecules substantially reduces the energy barrier between the two mutually-orthogonal elongated geometries (see Sec. III B). The suppression of this energy barrier yields stabilization of the D_{4h}-compressed coordination. The Rb$_2$CuCl$_4$(H$_2$O)$_2$ structure involves isolated JT-elongated CuCl$_4$(H$_2$O)$_2^{2-}$ complexes, whose equatorial plane (short-bonded ligands) is formed by two in-plane Cu-Cl bonds and the two out-of-plane Cu-OH$_2$ bonds (Fig. 1). As a result, the AFD structure can be easily suppressed due to the isolated character of the CuCl$_4$(H$_2$O)$_2^{2-}$ complex and the presence of water ligands. According to the PJT model, the strong axial-ligand field from water molecules favors the structural requirements to achieve the local structure changes from the initial D_{2h}-elongated geometry to the D_{4h}-compressed one. In the latter case, the two-shortest Cu-OH$_2$ bonds form the fourfold axis, whereas the four Cu-Cl bonds define a new CuCl$_4$ equatorial plane. This elongated-to-compressed structural change yields disappearance of the AFD structure and, consequently, the electronic ground-state related properties. Such a structural change can be achieved through either an increase of the axial ligand field or an increase of the electron-phonon coupling constant. In the former case, the replacement of H$_2$O ligands for the stronger axial-field NH$_3$ ligands leads directly to the tetragonal compressed CuCl$_4$(NH$_3$)$_2^{2-}$ complex.[32,33] Interestingly, both structural requirements can be achieved by applying pressure.

This work investigates the effect of pressure on Rb$_2$CuCl$_4$(H$_2$O)$_2$ through XRD and XAS in the 0–25 GPa

range. The presence of two water ligands exerts an axial compression favoring release of the JT distortion at moderate pressures, i.e., below the metallization pressure. This aspect is important in order to establish correlations between the crystal structure and, the electronic and vibrational structures from optical spectroscopy. Our aim is to elucidate whether the application of pressure mainly induces rotation of the CuCl$_4$(H$_2$O)$_2^{2-}$ D_{2h}-distorted octahedra or it is able to suppress the AFD structure. This latter case would modify the local structure from an elongated geometry to a compressed situation with four identical Cu-Cl bonds and the shortest Cu-O bond as fourfold axis. The searched transformation implies a modification of the electronic ground state with the unpaired electron changing from mainly $d_{x^2-y^2}$ to $d_{3z^2-r^2}$.[32–35]

II. EXPERIMENT

Single crystals of Rb$_2$CuCl$_4$(H$_2$O)$_2$ were grown by slow evaporation from alcoholic solutions following the procedure given elsewhere.[7]

The XAS experiments under pressure were performed at the absorption setup XAS10 of the D11 beamline at LURE (Orsay). The extended x-ray absorption fine structure (EXAFS) spectra of the investigated Rb$_2$CuCl$_4$(H$_2$O)$_2$ were measured at the Cu K-edge (E_0=8.98 keV) at room temperature using dispersive EXAFS in the 8.9–9.3 keV range. This experimental setup has been proved to be very sensitive for obtaining suitable EXAFS oscillations in a wavelength range where the diamond anvil absorption is very strong. XRD experiments under pressure were done in the energy dispersive setup WDIS of the DW11A beamline at LURE. The XRD and XAS data were analyzed by means of the FULL-PROF (Ref. 36) and the WINXAS package programs, respectively.

In both experiments the pressure was applied with a membrane-type diamond anvil cell employing silicon oil as pressure transmitter. The pressure was measured from the R-line shift of Ruby.

III. RESULTS AND DISCUSSION

A. Local and crystal structure of Rb$_2$CuCl$_4$(H$_2$O)$_2$

1. EXAFS and XRD analysis

Figure 1 shows the crystal structure of the Rb$_2$CuCl$_4$(H$_2$O)$_2$ and the corresponding anhydrous Rb$_2$CuCl$_4$. Note the different coordination geometry of Cu^{2+} in each structure as well as the distinct character of the AFD structure. In Rb$_2$CuCl$_4$(H$_2$O)$_2$, the Cu^{2+} complexes are isolated and do not share any common ligand in contrast to Rb$_2$CuCl$_4$.

The XRD and XAS data of Rb$_2$CuCl$_4$(H$_2$O)$_2$ at room temperature are given in Fig. 2 and Tables I and II. The results are compared with those of Rb$_2$CuCl$_4$. Apart from differences in XRD, which are associated with the tetragonal $P4_2/mnm$ [Rb$_2$CuCl$_4$(H$_2$O)$_2$] and the orthorhombic $Cmca$ (Rb$_2$CuCl$_4$) structures, a salient feature is the different XANES signal observed for each compound, which is re-
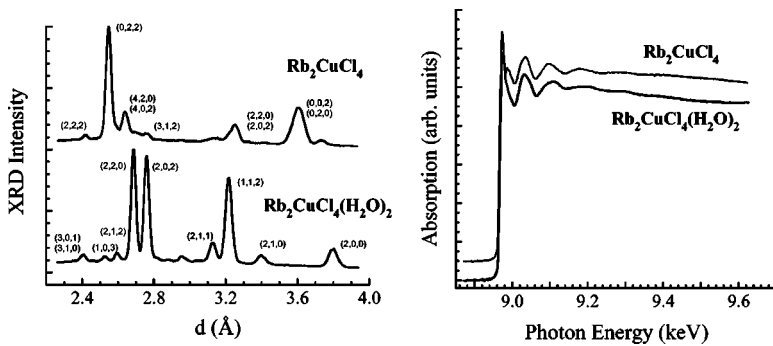
FIG. 2. XRD and XAS results obtained for $CuCl_4(H_2O)_2^{2-}$ and $CuCl_6^{4-}$ in $Rb_2CuCl_4(H_2O)_2$ ($P4_2/mnm$) and Rb_2CuCl_4 ($Cmca$), respectively, at ambient conditions.

lated to the different local structure around Cu^{2+} (Fig. 2, right).[34]

Figure 3 shows the variation of XAS and XRD of $Rb_2CuCl_4(H_2O)_2$ as a function of pressure. The corresponding variations of Cu-Cl and Cu-O bond lengths derived from XAS and the lattice parameters from XRD are plotted in Figs. 4(a) and 4(c). In Fig. 4(b), the variation of the complex volume with pressure is compared with the variation of the cell volume in order to analyze the local and crystal compressibility in $Rb_2CuCl_4(H_2O)_2$.

The analysis of the XRD data has been limited to the lattice cell parameters, i.e., the Bragg angles, since the measured peak intensity is inadequate for a proper Rietveld

TABLE I. Structural data of $Rb_2CuCl_4(H_2O)_2$ at ambient conditions. The lattice parameters and cell volume correspond to the tetragonal $P4_2/mnm$ space group. The reduced atomic coordinates and the metal-ligand bond distances around Cu^{2+} are included.

$a,b/Å$	$c/Å$	$V/Å^3$	Ref.
7.596(2)	8.027(3)	463.2(3)	31
7.597(19)	8.032(19)	464(3)	This work
Atomic coordinates	x	y	z
Cu	0	0	0
Rb	0	0.5	0.25
C11	0.7207	−0.7207	0
C12	0.2101	0.2101	0
O	0	0	0.2454
	Cu-L bond distances		
	Cu-C11:	3.000 Å	
	Cu-C12:	2.257 Å	
	Cu-O:	1.969 Å	

TABLE II. EXAFS fit parameters corresponding to the Cu K-edge ($E=8.98$ keV) in $Rb_2CuCl_4(H_2O)_2$ at ambient conditions (see Fig. 2).

Bond distance	N	$R/Å$	$\sigma^2/Å^2$
Cu-C11	2	2.85±0.15 Å	0.04±0.03
Cu-C12	2	2.25±0.05 Å	0.002±0.02
Cu-O	2	2.00±0.05 Å	0.003±0.02
		$S_0^2=0.66$	

analysis. Within the experimental accuracy, the energy-dispersive XRD diagrams of $Rb_2CuCl_4(H_2O)_2$ were explained according to the $P4_2/mnm$ crystal structure in the $0-15$ GPa range. Above 15 GPa, the splitting of the (220) Bragg peak evidences a structural phase transition. On the other hand, reliable variations of the local bond distances with pressure were obtained from the EXAFS oscillations according to the following procedure. First, we derive the Debye-Waller factors, the electron mean-free path parameter together with the Cu-Cl and Cu-O bond lengths of the $CuCl_4(H_2O)_2^{2-}$ complex at ambient pressure from the accurate ambient-pressure XAS using three neighbor shells (Fig. 2 and Table II). Secondly, we use the so-obtained parameters as input parameters for the next pressure XAS analysis. Due to the few EXAFS oscillations attained in diamond anvil cell (Fig. 3), an accurate XAS fit at a given pressure was accomplished allowing bond-distance variation but keeping the Debye-Waller and the electron mean-free path as fixed parameters.

Interestingly, the pressure behavior of complex and crystal shown in Fig. 4(b) is rather different. This phenomenon reflects the stiffness of the Cu-Cl and Cu-O bonds of the JT distorted complex, whose local compressibility is an order of magnitude smaller than the crystal compressibility. This conclusion is based on the different bulk modulus obtained by fitting the volume variations, $V_{Comp}(P)$ and $V_{Cryst}(P)$, with pressure to a Murnaghan equation of state [Fig. 4(b)]. Note that the error bar of V_{Comp} corresponds to the absolute error, which is an order of magnitude higher than the error of the volume change induced by pressure, $\Delta V = V_{Comp}(P) - V_{Comp}(0)$, i.e., EXAFS provides accurate distance variations (~ 0.01 Å) although the absolute errors for distance determinations may be significantly bigger. Therefore we obtain a local bulk modulus, $B_{loc}=240$ GPa, with an accuracy of about 10% taking the $V_{Comp}(0)$ value derived from x-ray data.

A similar result was found for $CuCl_6^{4-}$ in $[C_3H_7NH_3]_2CuCl_4$.[22] However, the abrupt change experienced by the long Cu-Cl distance at 15 GPa is noteworthy [Fig. 4(c)]. The XAS analysis reveals that the short Cu-Cl distance slightly increases with pressure ($\partial R/\partial P =0.0003$ Å GPa^{-1}) whereas the long Cu-Cl bond ($\partial R/\partial P= -0.008$ Å GPa^{-1}) reduces to a common distance, $R=2.27$ Å. This abrupt variation was evidenced by the divergence of the XAS fit using the D_{2h}-elongated $CuCl_4(H_2O)_2^{2-}$ complex distances as input parameters above 15 GPa. The fit provides axial Cu-Cl distances, which are physically meaningless
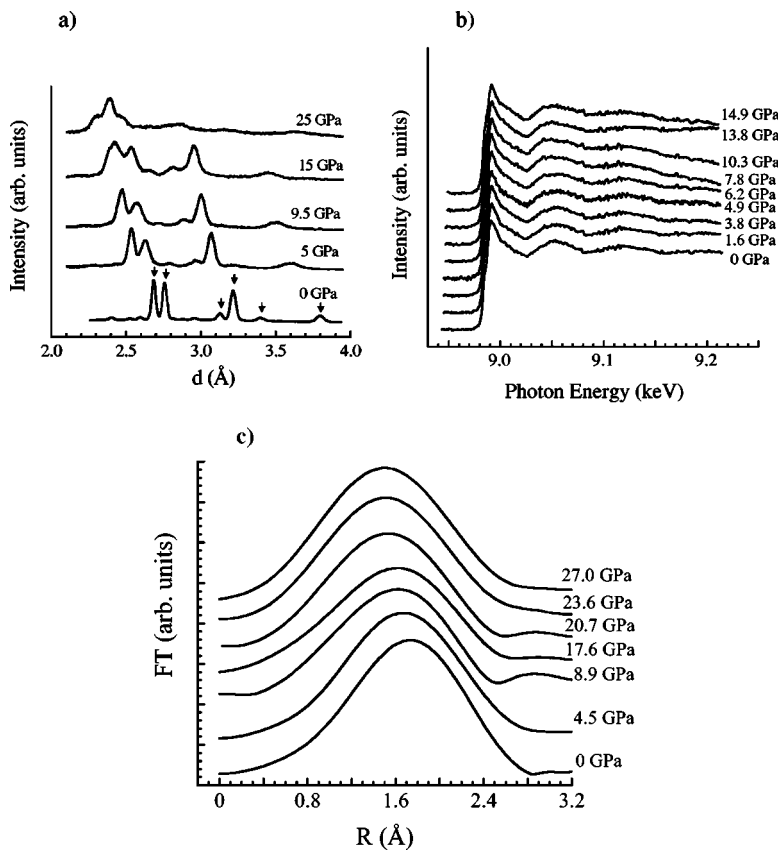
FIG. 3. Variation of XRD (a) and XAS (b) for $Rb_2CuCl_4(H_2O)_2$ as a function of pressure. Arrows in (a) indicate the Bragg peaks used for obtaining the lattice parameters given in Fig. 4(a). (c) Fourier transform (FT) of the EXAFS oscillations as a function of pressure. The corresponding bond distances, Cu-Cl and Cu-O, derived from the FT data are plotted in Fig. 4(c).

($R \geqslant 3$ Å). However, a fairly good convergence is obtained taking the compressed $CuCl_4(H_2O)_2^{2-}$ geometry as starting fit parameters. It must be noted that the compressed coordination geometry, which involves only two fit parameters, i.e., the Cu-Cl distance and the Cu-O distance, accounts for XAS in the 15–30 GPa range. Nevertheless, it fails for P <15 GPa, where only the elongated geometry with two different Cu-Cl distances and one Cu-O distance, provides suitable convergence.

We therefore associate the pressure-induced structural transformation at 15 GPa with the disappearance of the AFD structure, which is related to the suppression of the in-plane
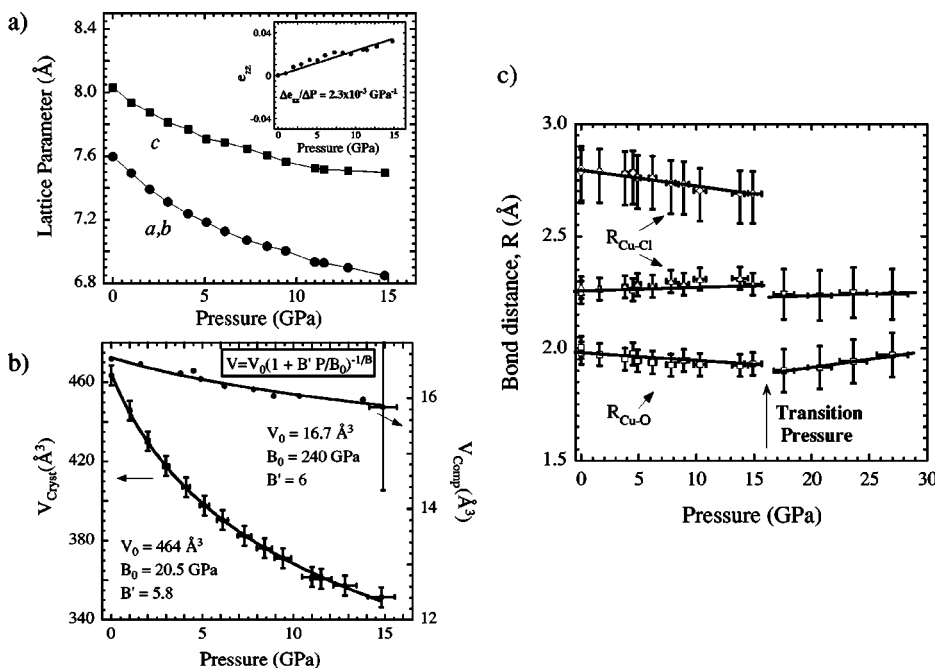

FIG. 4. (a) Variation of the lattice parameters, a, b, and c, and the strain parameter, $e_{zz}=\Delta c/c -\Delta a/a$, with pressure (see text). The point size contains the error bars. (b) Complex volume ($V_{Cu}=4/3R_1 \times R_2 \times R_3$) and crystal cell volume ($V=a^2c$) variation as a function of pressure. The solid lines correspond to the least-square fits to the Murnaghan's equation-of-state using $B_{loc}=240$ (30) GPa, and $B'_{loc}=6$ for the complex, and $B_0=20.5$ (8) GPa and $B'=5.8$ (2) for the crystal. (c) Distance variation of Cu-Cl (R_1 and R_2) and Cu-O (R_3) derived from XAS with pressure.

JT distortion. The Cu^{2+} coordination changes with pressure from an rhombic-elongated structure to a tetragonal-compressed situation. The associated bond distances change from 2.72 Å and 2.26 Å for Cu-Cl, and 1.97 Å for Cu-O, in the low-pressure phase, to 2.25 Å and 1.96 Å for Cu-Cl and Cu-O, respectively, in the high-pressure JT-suppressed phase. This change is also accompanied by a crystal phase-transition. It must be noted that we were not able to resolve the crystal space group above 16 GPa due to the poor XRD resolution, thus no structural data could be included in Fig. 4 in this pressure range. However, the complex volume experiences an abrupt jump of 16%; i.e., V_{comp} reduces from 16 $Å^3$ to 13.5 $Å^3$ at 16 GPa, thus approaching the variation of the crystal volume with pressure, in agreement what is expected in the high-pressure limit.

It is worth noting that pressure induces an increase of Cu-O distance above 16 GPa as 0.015 Å GPa^{-1}. This slight lengthening of the Cu-O bond together with the almost unmodified Cu-Cl bonds, $R_{Cu-Cl}=2.25$ Å, likely reflect an intra- to intermolecular charge-transfer electron, whose main effect is to soften the Cu-O bond.

2. Structural correlations and equation of state

The bulk modulus, B_0, and corresponding derivative, B', were obtained by fitting the measured complex and cell volumes to a Murnaghan's equation-of-state [Fig. 4(b)]. The comparison between variations of the crystal volume and the complex volume indicates that the complex is much less compressible ($B_0=240$ GPa; $B'=6$) than the crystal ($B_0=20.5$ GPa; $B'=5.8$). Furthermore, the lattice parameters vary differently with pressure. Parameters defining the FD plane, a and b, reduce with pressure slightly shorter than c, which is proportional to the interplanar distance. This behavior, which is shown in Fig. 4(a), reflects weakly pressure-induced crystal anisotropy. According to the PJT theory, the associated strain together with the isostatic reduction of the crystal volume can influence significantly the occurrence of the structural transition associated with the in-plane JT suppression and, therefore, the interplane AFD structure. In fact, crystal anisotropy and isostatic compression increase the effective axial stress along the O-Cu-O fourfold axis, yielding destabilization of the mainly x^2-y^2 hole state in favor of the $3z^2-r^2$ state. The associated structural change is accompanied by a reduction of the long axial Cu-Cl bonds towards a compressed complex. This behavior is precisely described within the PJT model, where the effects of the water molecules and crystal anisotropy are treated simultaneously through external axial-stress terms.

B. The pseudo-Jahn-Teller effect in the MX_4L_2 complex: Electron-phonon coupling $E \otimes e$, axial stress, and isostatic compression

1. Jahn-Teller model $E \otimes e$ in homonuclear MX_6 systems

The local coordination geometry of an octahedral MX_6 complex involving JT ions (M: Cu^{2+}, Cr^{2+}, Mn^{3+}, Ni^{3+} [low-spin configuration]) can be effectively treated on the basis of the electron-ion coupling, i.e., between the electronic state of

E_g symmetry and ligand-field distortions (either static or dynamic) related to e_g normal coordinates (JT $E \otimes e$ model). On the assumption that the complex distortion is either tetragonal (D_{4h}) or rhombic (D_{2h}), what is the usual case for the JT MX_6 complex, then the cubic-perturbed Hamiltonian can be described as a function of the octahedral e_g and a_{1g} normal coordinates of the X ligands within the harmonic approximation as[7,13]

$$H = H_{O_h} + \Delta H = H_{O_h} + \left(\frac{\partial H}{\partial Q_\theta}\right)_{Q_a=Q_\varepsilon=0} Q_\theta + \left(\frac{\partial H}{\partial Q_\varepsilon}\right)_{Q_a=Q_\theta=0} Q_\varepsilon$$
$$+ \frac{1}{2}k_{a_{1g}}Q_{a_{1g}}^2 + \frac{1}{2}k_e(Q_\theta^2 + Q_\varepsilon^2), \tag{1}$$

where H_{O_h} is the cubic Hamiltonian at the equilibrium geometry, $R=R_0$, and ΔH is the Hamiltonian perturbation. The normal coordinates are defined as follows:

$$Q_{a_{1g}} = \sqrt{6}\left[\frac{1}{3}(R_{ax} + R_{eq1} + R_{eq2}) - R_0\right],$$

$$Q_\theta = \frac{2}{\sqrt{3}}(R_{ax} - R_{eq}),$$

$$Q_\varepsilon = R_{eq2} - R_{eq1},$$

where R_{ax} is the axial M-X distance of an elongated octadron complex, $R_{eq} = \frac{1}{2}(R_{eq1}+R_{eq2})$ is the average of the two equatorial distances and R_0 is the average M-X distance. Within the $E \otimes e$ JT theory, the parameter $\rho = \sqrt{Q_\theta^2 + Q_\varepsilon^2}$ describes the radius of distortion in $(Q_\theta, Q_\varepsilon)$-space in the six-coordinate complex.[1,2,7,13]

The representation matrices of ΔH for the parent octahedral $T_{2g}(xy, xz, yz)$ and $E_g(3z^2-r^2, x^2-y^2)$ states are then given by

$$\langle \Delta H \rangle = \frac{1}{\sqrt{6}}A_1^t \begin{pmatrix} 2Q_\theta & 0 & 0 \\ 0 & -Q_\theta + \sqrt{3}Q_\varepsilon & 0 \\ 0 & 0 & -Q_\theta - \sqrt{3}Q_\varepsilon \end{pmatrix}$$

for T_{2g} and,

$$\langle \Delta H \rangle = \frac{1}{2}A_1^e \begin{pmatrix} -Q_\theta & Q_\varepsilon \\ Q_\varepsilon & Q_\theta \end{pmatrix} \tag{2}$$

for E_g.

The parameter $A_1^i (i=e,t)$ is the linear JT electron-ion coupling coefficient, which is quite different for the e_g and t_{2g} one-electron wave functions (or analogously the T_{2g} and E_g states).[14] Note that A_1^e as defined in Eq. (2) is one-half the corresponding linear coupling constant employed elsewhere.[1,2]

If we limit our analysis to the E_g state ($E \otimes e$ model), and we introduce the polar coordinates, ρ and α defined as $Q_\theta = \rho \cos(\alpha)$ and $Q_\varepsilon = \rho \sin(\alpha)$, then the energy becomes

$$E_\pm = \pm \frac{1}{2}A_1^e \rho + \frac{1}{2}k_e \rho^2.$$

The $\pm$ refers to the $B_{1g}(x^2-y^2)$ and $A_{1g}(3z^2-r^2)$ states in elongated D_{4h}, and an appropriate combination of
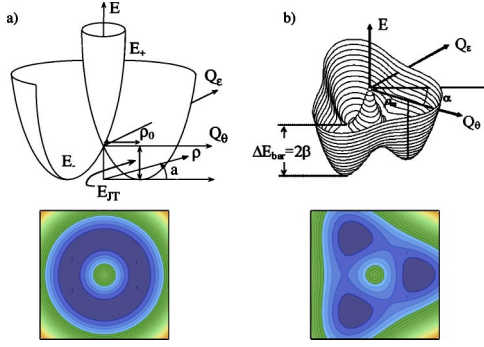
FIG. 5. (Color online) (a) Ground-state energy surface and projection in $(Q_\theta, Q_\varepsilon)$-space, corresponding to the $E \otimes e$ Jahn-Teller (JT) effect for MX_6 octahedral complex in the linear approximation $(A_3 = A_2 = 0)$: Mexican hat surface. (b) Ground-state energy-surface and corresponding projection including JT second-order $(A_2 \neq 0)$ and anharmonic $(A_3 < 0)$ terms. Note the formation of three-equivalent potential wells (warped Mexican hat surface: Tricorn). The parameters involved in the $E \otimes e$ JT model are indicated.

both states in D_{2h}. The B_{1g} stabilization energy is just the JT energy, which is given within this scheme by $E_{JT} = -\frac{1}{4} A_1^e \rho_0$. Where $\rho_0 = A_1^e / 2k_e$ with $k_e = \mu \omega^2$ (Refs. 7 and 13) corresponds to the equilibrium geometry of the E_- surface [Fig. 5(a)]. In first-order electron-ion terms, the ground-state energy-surface in $(Q_\theta, Q_\varepsilon)$-space is the well-known Mexican hat potential energy surface. In this approximation, it corresponds to any point around the $(Q_\theta, Q_\varepsilon)$-space circumference of radius ρ_0. This means that structures going from the axially elongated octahedron $(Q_\theta = \rho_0, Q_\varepsilon = 0)$ to the axially compressed octahedron $(Q_\theta = -\rho_0, Q_\varepsilon = 0)$, passing through different tetragonal and rhombic intermediate structures $(Q_\theta \neq 0, Q_\varepsilon \neq 0)$, are equally probable provided that the $M\text{-}X_i$ distance deviations, $\Delta R_i = R_i - R_0$ $(i = 1 - 6)$, verify

$$\rho = \rho_0 = \sqrt{\sum_{i=1}^{6} \Delta R_i^2}.$$

Obviously the linear approximation does not reflect any real situation. Actual coordination geometries are accounted for within this model including second-order JT terms and anharmonicity in Eq. (1). These terms are given, respectively, by

$$A_2(Q_\theta^2 - Q_\varepsilon^2) + 2A_2 Q_\theta Q_\varepsilon = A_2 \rho^2 [\cos(2\alpha) + \sin(2\alpha)],$$

$$A_3[Q_\theta^3 - 3Q_\theta Q_\varepsilon^2] = A_3 \rho^3 \cos^3(3\alpha) \text{ with } A_3 < 0. \quad (3)$$

The energy is thus given by diagonalizing the matrix[5,20,26]

$$\begin{bmatrix} -A + B & C \\ C & A + B \end{bmatrix}$$

with

$$A = \frac{1}{2} A_1^e \rho \cos(\alpha) + \frac{1}{2} k_e \rho^2 + A_2 \rho^2 \cos(2\alpha),$$

$$B = A_3 \rho^3 \cos(3\alpha),$$

$$C = \frac{1}{2} A_1^e \rho \sin(\alpha) + A_2 \rho^2 \sin(2\alpha). \quad (4)$$

The presence of only anharmonic terms $(A_2 = 0; A_3 \neq 0)$, is enough to account for the usual elongated-octahedron geometries of D_{4h}, or nearly D_{4h}, usually found in JT systems. The ground-state energy-surface is then given by

$$E_{gs} = -\frac{1}{2} A_1^e \rho + \frac{1}{2} k_e \rho^2 + A_3 \rho^3 \cos(3\alpha). \quad (5)$$

Equation (5) corresponds to a warped Mexican hat surface with three equivalent minima at $(Q_\theta = \rho_0, Q_\varepsilon = 0)$, $(Q_\theta = -\frac{1}{2}\rho_0, Q_\varepsilon = (\sqrt{3}/2)\rho_0)$, and $(Q_\theta = -\frac{1}{2}\rho_0, Q_\varepsilon = -(\sqrt{3}/2)\rho_0)$, respectively, whose solutions fulfills the condition: $\sin(3\alpha) = 0$ [Fig. 5(b)], and

$$\rho_m = \frac{A_1^e}{2k_e} - 6\frac{A_3}{A_1^e}\left(\frac{A_1^e}{2k_e}\right)^2 = \rho_0\left(1 - 3\frac{A_3 \rho_0^2}{A_1^e}\right),$$

which is similar to ρ_0 when $A_1^e \gg A_3 \rho_0^2$.

It is worth mentioning that although each minimum represents a local D_{4h}-symmetry complex, the system keeps the overall cubic symmetry. In dynamical JT systems, the time-averaged symmetry is cubic, while for static JT systems, the cubic symmetry is related to the averaged symmetry of the three-equivalent statically-distorted JT complexes along x, y, and z (topological degeneracy). Thus the criterion for static and dynamic JT regimes relies on the experiment time scale. Within this model, the mean jumping time of the system among the three equivalent minima is proportional to the overlap between vibronic wave functions centered in the three minima. Therefore, the occurrence of a given JT regime strongly depends on the separation of the minima in $(Q_\theta, Q_\varepsilon)$-space, the vibrational e_g-mode energy and the energy barrier between wells, i.e., the energy difference between minima and saddle points. This latter energy is according to Eq. (5) given approximately by $\Delta E_{act} = 2\beta$ with

$$\beta \approx |A_3| \rho_0^3 \approx |A_3| \left[\frac{A_1^e}{2\mu\omega^2}\right]^3. \quad (6)$$

Note that only anharmonic terms have been considered in this equation.

JT distortions of rhombic or compressed octahedron symmetry can also be explained on the basis of present model, but including second-order JT terms in the Hamiltonian [Eq. (4)]: $A_2 \neq 0$. The competition between A_2 and A_3 parameters finally determines the JT complex distortion. In this context, it must be noted that whereas both elongated and compressed geometries have been observed for CuF_6 (Refs. 3–6,26,35,37) and CuO_6,[1,38] a compressed coordination has never been so far observed in $CuCl_6$, whose coordination geometries correspond to elongated nearly-D_{4h}. Unfortunately, the criterion to predict whether a complex will exhibit a given coordination geometry is still unsolved in spite of the efforts carried out to explain the microscopic dependence of A_2 and A_3 with the complex structure through density functional theory (DFT) calculations.[39]
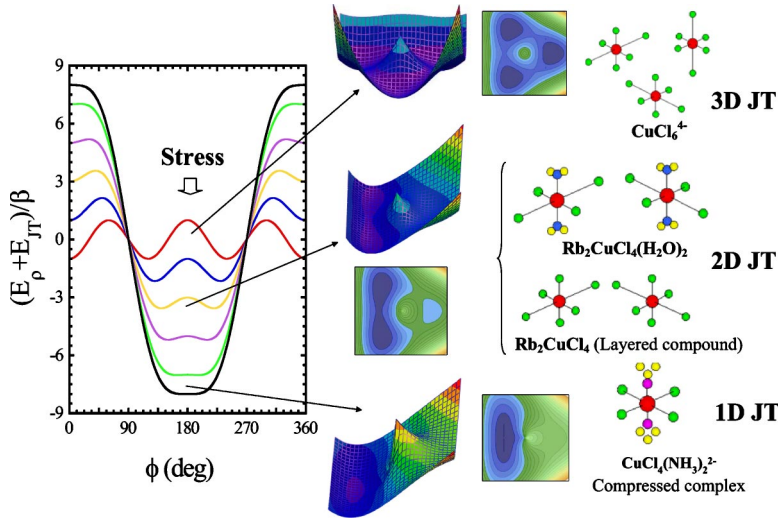
FIG. 6. (Color online) Effect of the axial stress in the ground-state energy in $(Q_\theta, Q_\varepsilon)$-space. The effective axial stress produced by the axial ligands in homo- and heteronuclear MX_4L_2 systems ($X=Cl$; $L=Cl, H_2O, NH_3$) is indicated with the associated coordination geometries. The $(Q_\theta, Q_\varepsilon)$-space ground-state energy surface is shown on the left. Note the evolution from elongated-to-compressed coordination geometry upon increasing the axial stress. The collapse into the compressed geometry takes place at $S_{crit}=9\beta$. The $CuCl_4L_2$ series ($L=Cl \to H_2O \to NH_3$) illustrates the effect of axial stress induced by crystal anisotropy (homonuclear) or axial ligand-field (heteronuclear) in real complexes at ambient conditions.

2. Pseudo-Jahn-Teller model in heteronuclear MX_4L_2

The present $E \otimes e$ model can also be applied for heteronuclear complexes, MX_4L_2, on the basis that the L-ligand effects with respect to the homonuclear MX_6 complex, are described by an effective axial-stress term whose tetragonal and rhombic components are $\frac{1}{2}A_1^e\rho_s \cos(\alpha_s)$ and $\frac{1}{2}A_1^e\rho_s \sin(\alpha_s)$.[1,26,37] The addition of the axial-stress term in A and C [Eq. (4)] leads to the so-called PJT model.[26,43] The achievement of PJT theory has been checked in different Cu^{2+} complexes like $CuCl_6^{4-}$, $CuCl_4(H_2O)_2^{2-}$, $CuCl_4(NH_3)_2^{2-}$ for explaining the variation of the gyromagnetic-tensor components with temperature.[40,41] Furthermore, the introduction of an axial-stress term in Eqs. (4) is useful to deal simultaneously with either homo- or heteronuclear complexes under external axial compression, hydrostatic pressure or low-symmetry crystal-field strains associated with the crystal anisotropy. Thus Eq. (5) transforms to

$$E_{gs} = -E_{JT} - \beta \cos(3\alpha) - S \cos(\alpha - \alpha_s), \qquad (7)$$

where E_{JT} is the JT energy, $\beta \approx A_2\rho_0^2 + |A_3|\rho_0^3$ and $S = \frac{1}{2}A_1^e\rho_s$. The parameters ρ_s and α_s indicate the stress-induced deformation, due to the crystal anisotropy or the nonoctahedral ligand field in heteronuclear complexes. Experimental values of β vary from near zero for Cu^{2+}-doped MgO, 5–10 meV for Cu^{2+}-doped ZnF_2, and 35–75 meV for $CuCl_6^{4-}$ and $Cu(H_2O)_6^{2+}$ (Refs. 35,40,41). The linear electron-ion coupling parameter, A_1^e, was also determined experimentally for $CuCl_6^{4-}$ ($A_1^e=2.25$ eV Å^{-1}) (Ref. 8) and MnF_6^{3-} ($A_1^e=5.2$ eV Å^{-1}).[14]

Figure 6 shows the effect of applying a compressive stress along the X-M-X axis ($\alpha_s=\pi$) starting from an elongated-D_{4h} situation ($S=0$) for the homonuclear MX_6 complex. The stress gradually destabilizes the potential well, which is associated with the axially elongated M-X bond pointing along the stress, with respect to the other two wells. The stress range, $0<S<9\beta$, corresponds to the two-dimensional JT regime (2D). As Fig. 6 shows, the potential-well destabilization is accompanied by a decrease of the energy barrier, ΔE_{act}, connecting the two equivalent ground-state wells, from $\Delta E_{act}=2\beta$ for $S=0$ (elongated octahedron) to $\Delta E_{act}=0$

for $S=9\beta$ (compressed octahedron coordination).

The AFD structure displayed by layered perovskites A_2CuCl_4 (Ref. 8) and $AMnF_4$ (Ref. 14) (A: monovalent ion) are examples of two-dimensional JT regimes (Figs. 1 and 6). In these systems, the layered-crystal anisotropy provides the axial-stress field. Interestingly, further increase of the axial stress around 9β causes a progressive approach of the two ground-state wells in $(Q_\theta, Q_\varepsilon)$-space for $S=9\beta$ (Fig. 6). Above this critical value, the two wells collapse into a single well at $\rho \approx \rho_0$ and $\alpha=\pi$, which corresponds to the compressed-D_{4h} complex, whose fourfold X-M-X axis is along the stress. In terms of electron-ion interaction, the stress increases the electronic repulsion in the $3z^2$-r^2 orbital making the electronic ground state to be mixed between x^2-y^2 and $3z^2-r^2$. Further increase of S reduces the stressed M-X bond distance, yielding destabilization of the $3z^2-r^2$ with respect to the x^2-y^2 along the transition from elongated to compressed D_{4h}.

In general, the structural-change sequence shown in Fig. 6 can be adapted for $CuCl_4L_2$ ($L=Cl, H_2O, NH_3$) complex. The L-ligands exert an axial stress, whose value increases along the sequence $L=Cl \to H_2O \to NH_3$. Consequently, the associated coordination geometries correspond to 3D elongated-JT octahedron along either Cl-Cu-Cl direction (D_{4h}),[27,28] 2D elongated-JT along either two Cl-Cu-Cl directions (D_{2h}) (Refs. 7,23,29,33) and, 1D compressed-JT along H_3N-Cu-NH$_3$ (D_{4h}),[32,33] respectively (Fig. 6).

3. Elongated-to-compressed transition in MX_4L_2: Pressure estimates

The external stress, either axial or hydrostatic, within a given complex can lead to similar coordination-geometry variations. However, there is no evidence of such structural changes at a local level using external stress, in spite of the intense work devoted to achieve such a goal. In the case of homonuclear complexes, it is likely due to the high-pressure requirements to attain the critical stress $S_{crit}=9\beta$. In A_2CuCl_4, the critical pressure was estimated above 30 GPa.[22] Nevertheless, the elongated-to-compressed structural change can be easier tackled in hydrostatic pressure

experiments provided that we start from an axially-stressed complex like $CuCl_4(H_2O)_2$. Moreover, the parameters associated with the potential energy surface of this complex are known from electron paramagnetic resonance (EPR) experiments.[41] They are $S_{H_2O}=25$ meV and $\beta=12$ meV for $CuCl_4(H_2O)_2$ at ambient conditions ($S_{D_2O}=70$ meV for the deuterated complex).[42] It implies that an external axial stress localizes the surface minimum at a compressed tetragonal geometry ($\alpha=\pi$) whether the condition $S_{ext}>9\beta$ is fulfilled. This requirement can be achieved by applying hydrostatic pressure due to either an enhancement of the axial stress induced by pressure in anisotropic crystals, or by decreasing the energy barrier, 2β, in nearly isotropic systems. The pressure-induced axial stress is inversely proportional to the Cu-O distance provided that the pressure produces a nearly isostatic strain in the complex. In fact, this is the case since the relative decrease of the a and c lattice parameters is: $\Delta c/c \approx \Delta a/a$ [inset of Fig. 4(a)]. Consequently, the water molecules provide an axial stress that can be estimated on the basis of the stress value at ambient conditions ($R_{Cu-O}=1.97$ Å) and the pressure-induced axial-stress, through

$$S_{ext}(P)=S_{ext}\left(\frac{c_0}{c(P)}\right)^m, \qquad (8)$$

where c_0 and $c(P)$ are the lattice parameter at ambient pressure and P, respectively, and $S_{ext}=25$ meV is the effective axial stress due to H_2O at ambient pressure.[41] Note that this expression is valid on the assumption that the water stress is proportional to the interatomic distance reduction along the Cu-O bond direction, thus the crystal strain along c. According to XRD data (Fig. 4) and crystal-field theory ($m\approx3-5$),[43,46] we estimate an axial stress at 15 GPa of $S_{ext}(15)=31-36$ meV. This value is still far from the critical stress: $S_{crit}=9\beta=108$ meV, provided that β does not change appreciably with pressure. However, the latter condition is hard to concile in high-pressure experiments since, according to Eq. (6), the energy barrier mainly depends on the equilibrium coordinate, ρ_m, hence on the complex volume. In fact, a main effect of hydrostatic pressure on $CuCl_4(H_2O)_2^{2-}$ is to reduce the energy barrier. We can roughly estimate its pressure dependence following Eq. (6). The β parameter relies mainly on the electron-ion coupling, A_1^e, and the e_g-vibration frequency, ω. Both parameters depend on the crystal-volume as $A_1^e=A_1^e(0)(V_0/V)^n$ and $\omega=\omega_0(V_0/V)^\gamma$, where $A_1^e(0)$, V_0, and ω_0 are the electron-ion coupling parameter, the volume, and the phonon frequency at zero pressure, respectively, and n is an exponent close to 1 (see below), and γ is the Grüneisen parameter. Therefore, we obtain

$$\beta \propto \rho_0^3 \propto \left(\frac{A_1^e}{\omega^2}\right)^3 \propto \left(\frac{V_0}{V}\right)^{3(n-2\gamma)}$$

or, analogously,

$$\beta(P)=\beta(0)\left(\frac{V_0}{V}\right)^{3(n-2\gamma)} \qquad (9)$$

with $\beta(0)=12$ meV at ambient pressure. Therefore, the critical stress, $S_{crit}=9\beta$, decreases with pressure if $n<2\gamma$. Although $\beta(P)$ is difficult to calculate[5] since the n and γ exponents are not known for $Rb_2CuCl_4(H_2O)_2$, we can roughly estimate it taking the equation-of-state (Fig. 4), and the exponents usually found in other JT systems: $n\approx1$ (Refs. 13,40) and $\gamma\approx1$.[41,44,45] So that we obtain $\beta(15)=\beta(0)[465/350]^{-3}=5.1$ meV and, consequently, the critical stress reduces to $S_{crit}=9\beta=46$ meV at 15 GPa.

Precisely, we can obtain the critical pressure, P_{crit}, on the basis of Eqs. (8) and (9). At P_{crit}, c and V must verify the structural constraint $c_0/c(P_{crit})=1.63(V/V_0)$. According to the equation-of-state of $Rb_2CuCl_4(H_2O)_2$ (Fig. 4), that condition yields a critical pressure: $P_{crit}\approx20$ GPa. Although this value strongly depends on the particular choice of n and γ, the present estimate provides a fair agreement with the experimental critical pressure, $P=16$ GPa (Fig. 4).

It is worth noting that the experimental critical pressure in $Rb_2CuCl_4(H_2O)_2$ is one-half the estimated critical pressure for $CuCl_6^{4-}$ in A_2CuCl_4.[22] Within PJT model this difference is likely due to the larger β value (≈50 meV) and the weaker axial stress attained in homononuclear complexes, even in anisotropic crystals. Both effects yield larger strain and higher pressure conditions to achieve the change of coordination geometry in $CuCl_6^{4-}$.

A complete structural study on the pressure-induced variation of the coordination geometry in layered perovskites A_2CuCl_4 ($A=Rb$, R-NH_3: R-alkyl groups) is currently in progress.

IV. CONCLUSIONS

Throughout this work, we demonstrate that the JT distortion in Cu^{2+} can be efficiently suppressed in axially-stressed complexes. In the present case, this situation is attained through the heteronuclear $CuCl_4(H_2O)_2^{2-}$ complex, whose water ligands favor the elongated-to-compressed local-structure transformation at moderate pressures. In fact, water molecules provide an intermediate axial ligand-field between that attained in the homonuclear $CuCl_6^{4-}$ complex, associated with an x^2-y^2 unpaired electron, and the heteronuclear tetragonal-compressed $CuCl_4(NH_3)_2^{2-}$ complex with $3z^2-r^2$ ground state. The ammonium axial ligand-field leads directly to a D_{4h}-compressed coordination beyond 2D JT elongated-distortion associated with the Cl ligands. High hydrostatic pressure on $Rb_2CuCl_4(H_2O)_2$ favors an increase of the axial strain along the Cu-O bond, yielding stabilization of the D_{4h}-compressed $CuCl_4(H_2O)_2^{2-}$ coordination geometry. The observed structural change can be explained within the PJT model, assuming that the hydrostatic pressure exerts an increasingly axial strain along c favored by the crystal anisotropy. Finally, this work clearly demonstrates the adequacy of the PJT model to explain the structural variation found through XAS and XRD techniques, and highlights the usefulness of heteronuclear complexes to achieve the foreseen elongated-to-compressed structural changes.

---

*Author to whom correspondence should be addressed. E-mail address: rodriguf@unican.es

[1] D. Reinen and M. Atanasov, Magn. Reson. Rev. **15**, 167 (1991).

[2] M. A. Hitchman, Comments Inorg. Chem. **15**, 197 (1994).

[3] M. J. Riley and M. A. Hitchman, Inorg. Chem. **28**, 3926 (1989).

[4] M. J. Riley, L. Dubicki, G. Moran, E. R. Krausz, and I. Yamada, Chem. Phys. **145**, 363 (1990).

[5] G. Steffen, D. Reinen, H. Stratemeier, M. J. Riley, M. A. Hitchman, H. E. Mathies, K. Recker, F. Wallrafen, and R. Niklas, Inorg. Chem. **29**, 2123 (1990).

[6] D. Reinen, G. Steffen, M. A. Hitchman, H. Stratemeier, L. Dubicki, E. R. Krausz, M. J. Riley, H. E. Mathies, K. Recker, and F. Wallrafen, Chem. Phys. **155**, 117 (1991).

[7] R. Valiente and F. Rodríguez, J. Phys. Chem. Solids **57**, 571 (1996).

[8] R. Valiente and F. Rodríguez, Phys. Rev. B **60**, 9423 (1999).

[9] D. Oelkrug, Struct. Bonding (Berlin) **9**, 1 (1971).

[10] W. Massa and J. Steiner, J. Solid State Chem. **32**, 137 (1980).

[11] F. Palacio and M. C. Morón, in *Research Frontiers in Magnetochemistry*, edited by C. J. O'Connor (World Scientific, Singapore, 1993).

[12] F. Rodríguez, P. Núñez, and M. C. Marco de Lucas, J. Solid State Chem. **110**, 370 (1994).

[13] F. Aguado, F. Rodríguez, and P. Núñez, Phys. Rev. B **67**, 205101 (2003).

[14] F. Rodríguez and F. Aguado, J. Chem. Phys. **118**, 10 867 (2003).

[15] P. Day, A. K. Gregson, and D. H. Leech, Phys. Rev. Lett. **30**, 19 (1973).

[16] H. D. Lutz, M. Schneider, and C. Wickel, Z. Kristallogr. **211**, 8 (1996).

[17] C. Dobe, H. P. Andres, and P. L. W. Tregenna-Piggott, Chem. Phys. Lett. **362**, 387 (2002).

[18] F. S. Ham, Phys. Rev. **166**, 307 (1968).

[19] M. C. M. O'Brien, Phys. Rev. **187**, 407 (1969).

[20] J. S. Griffith, *The Theory of Transition Metal Ions* (Cambridge University Press, Cambridge, 1980).

[21] F. Aguado, F. Rodríguez, R. Valiente, A. Señas, and I. Goncharenko, J. Phys.: Condens. Matter **16**, 1927 (2004).

[22] F. Rodríguez, M. Hanfland, J. P. Itiè, and A. Polian, *Frontiers of High Pressure Research II. Application of High Pressure to Low-Dimensional Novel Electronic Materials* (Kluwer Academic, Dordrecht, 2001),Vol. 48, p. 143.

[23] Y. Moritomo and Y. Tokura, J. Chem. Phys. **101**, 1763 (1994).

[24] I. Loa, P. Adler, A. Grzechnik, K. Syassen, U. Schwarz, M. Hanfland, G. Kh. Rozenberg, P. Gorodetsky, and M. P. Pasternak, Phys. Rev. Lett. **87**, 125501 (2001).

[25] L. Pinsard-Gaudart, J. Rodríguez-Carvajal, A. Daoud-Aladine, I. Goncharenko, M. Medarde, R. I. Smith, and A. Revcolevschil, Phys. Rev. B **64**, 064426 (2001).

[26] M. J. Riley, M. A. Hitchman, and D. Reinen, Chem. Phys. **102**, 11 (1986).

[27] R. H. Borcherts, H. Kanzaki, and H. Abe, Phys. Rev. B **2**, 23 (1970).

[28] R. Valiente, Ph.D. thesis, Universidad de Cantabria, 1998.

[29] R. Valiente, L. M. Lezama, F. Rodríguez, and M. Moreno, Mater. Sci. Forum **239**, 729 (1997).

[30] B. Baticle, F. Rodríguez, and R. Valiente, Radiat. Eff. Defects Solids **135**, 89 (1995).

[31] K. Waizumi, H. Masuda, and H. Ohtaki, Acta Crystallogr., Sect. C: Cryst. Struct. Commun. **C48**1374 (1992).

[32] F. Boettcher and J. M. Spaeth, Phys. Status Solidi B **61**, 465 (1974).

[33] A. G. Breñosa, M. Moreno, F. Rodríguez, and M. Couzi, Phys. Rev. B **44**, 9859 (1991).

[34] N. Kosugi, T. Yokoyama, K. Asakura, and H. Kuroda, Chem. Phys. **91**, 249 (1984).

[35] K. Finnie, L. Dubicki, E. R. Krausz, and M. J. Riley, Inorg. Chem. **29**, 3908 (1990).

[36] J. Rodríguez-Carvajal, FULLPROF Program,V. 3.5d, 1988.

[37] D. Reinen, and S. Krause, Inorg. Chem. **20**, 2750 (1981).

[38] J. Bebendrof, H. Bürgi, E. Gamp, M. A. Hitchman, A. Murphy, D. Reinen, M. J. Riley, and H. Stratemeier, Inorg. Chem. **35**, 7419 (1996).

[39] J. A. Aramburu, M. T. Barriuso, P. Hernandez, and M. Moreno, Adv. Quantum Chem. **44**, 445 (2003), and (private communication).

[40] D. Reinen and M. A. Hitchman, Z. Phys. Chem. (Munich) **200**, 11 (1997).

[41] M. J. Riley, M. A. Hitchman, D. Reinen, and G. Steffen, Inorg. Chem. **27**, 1924 (1988).

[42] C. Dobe, H. P. Andres, P. L. W. Tregenna-Piggott, S. Mossin, H. Weihe, and H. Janssen, Chem. Phys. Lett. **362**, 387 (2002).

[43] P. Núñez, J. Ruiz-Morales, A. Lozano-Gorrín, P. Gili, V. Rodríguez, J. González-Platas, M. T. Barriuso, and F. Rodríguez, J. Chem. Soc. Dalton Trans. **2**, 273.(2004).

[44] J. R. Ferraro, *Vibrational Spectroscopy at High External Pressures: The Diamond Anvil Cell*, (Academic, Orlando, 1984).

[45] W. B. Holzapfel and N. S. Isaacs, *High-Pressure Techniques in Chemistry and Physics. A Practical Approach* (Oxford University Press, New York, 1997).

[46] A. B. P. Lever, *Inorganic Electronic Spectroscopy* (Elsevier, Amsterdam, 1984).